Sensors and Actuators B 145 (2010) 386–393

Contents lists available at ScienceDirect

Sensors and Actuators B: Chemical

journal homepage: www.elsevier.com/locate/snb

The humidity-sensitive property of MgO-SBA-15 composites in one-pot synthesis

Rui Wang[a], Xiangwei Liu[a], Yuan He[a], Qing Yuan[b], Xiaotian Li[b], Geyu Lu[a], Tong Zhang[a,*]

[a] State Key Laboratory on Integrated Optoelectronics, College of Electronic Science and Engineering, Jilin University, Changchun 130012, China
[b] Department of Material Science and Engineering, Jilin University, Changchun 130012, China

ARTICLE INFO

Article history:
Received 25 April 2009
Received in revised form
11 December 2009
Accepted 12 December 2009
Available online 22 December 2009

Keywords:
MgO-SBA-15
Humidity sensor
Complex impedance
Sensing mechanism

ABSTRACT

MgO-SBA-15 has been successfully developed as a kind of humidity-sensitive material. The structure of MgO-SBA-15 materials was characterized by XRD, IR spectroscopy, N_2 adsorption–desorption, TEM and XPS. The study proved that the MgO did not destroy the mesoporous structure of SBA-15 via the characteristic results of XRD and N_2 adsorption–desorption. Researchers built the thick film humidity sensors on the Al_2O_3 ceramic substrate with two Ag–Pd interdigital electrodes with five fingers. The sensor shows excellent humidity sensitivity from 11% to 95%RH, and it has very good response and recovery property. The response time is about 10 s and the recovery time is about 20 s. We found that the mesoporous structure of the sensing materials contributed to the humidity sensitivity. We discussed a possible mechanism based on the humidity sensor produced by MgO-SBA-15.

1. Introduction

Humidity sensors have been used in an increasing number of applications in industrial processing and environmental control. Growing demands for controlling water vapor have led to considerable interest in the development of sensing materials [1–5]. A variety of materials have been used to prepare humidity sensors, such as ceramics [6–8], conductive polymers [9–14], and metal oxide [15–20]. The techniques selected to fabricate sensors include thin film techniques [21–22] and thick film techniques [23–25]. Using any of these materials and techniques, the operating principles are based on the resistive, capacitive, or impedance conductivity properties of the sensing materials. Ceramics have shown desirable properties such as chemical and thermal stability, environmental adaptability, and applicability at high temperatures. But ceramics need to be heated to wash out moisture. Conductive polymers can usually stay in good working order in humidity, but they have an undesirable water-resistant property under circumstances involving high RH, and at high temperatures, they cannot work as usual.

Since a family of novel mesoporous silica materials called M41S was synthesized by the scientists from Mobil Oil Corporation, mesoporous silica materials have been receiving wide attention from both the scientific and industrial communities [26,27]. The large surface area created by mesoporous materials [28–31] enables an improvement in the water vapor adsorption properties of humidity devices. In our previous works, we have reported the humidity-sensitive properties of LiCl doped SBA-15 [32,33] and LiCl doped SBA-16 [34]. But the amount of LiCl is reduced when dissolved into water, due to its water-solubility. Sometimes, LiCl reacted with the mesoporous wall during the material preparing process, and the mesoporous structure was destroyed [32]. In order to resolve these problems, we selected metal oxide MgO and loaded it into SBA-15 to develop the humidity sensor. MgO is usually used as a functional component in different fields [19,35]. In this paper, we synthesize MgO-SBA-15 composites in one-pot method and investigate its humidity-sensitive property based on this material. This method does not destroy the mesoporous structure, and the obtained material has a very good response to variations in environmental humidity.

2. Experimental

2.1. Preparations of SBA-15 and MgO-SBA-15

We prepared mesoporous silica SBA-15 according to the method reported by Li and Zhao [36]. The detailed procedure was as follows: first, 2 g P123 ($EO_{20}PO_{20}EO_{20}$) as a template was dissolved in 60 ml HCl solution at room temperature. Then, 4.25 g tetraethyl orthosilicate (TEOS) was added dropwise under stirring at 40 °C for 24 h. Subsequently, the resulting mixture was aged at 40 °C for 24 h without stirring. The final aqueous solution was transferred into a Teflon-lined stainless steel autoclave, sealed tightly, and treated hydrothermally at 100 °C for 24 h. The autoclave was

* Corresponding author. Tel.: +86 431 85168385; fax: +86 431 85168385.
E-mail addresses: zhangtong@jlu.edu.cn, heyuan@jlu.edu.cn, wangrui1215@163.com (T. Zhang).

0925-4005/$ – see front matter.
doi:10.1016/j.snb.2009.12.025

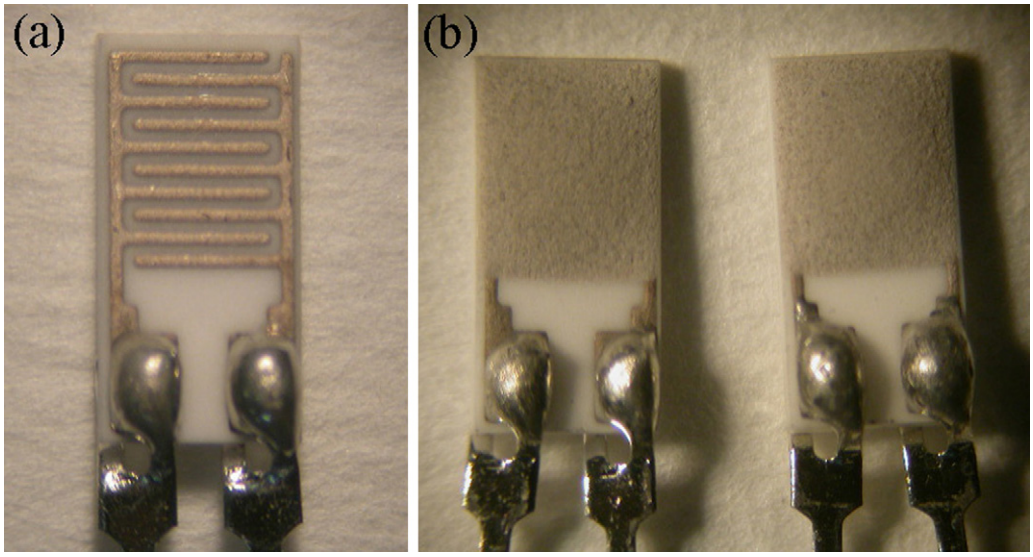

Fig. 1. Photograph of (a) the blank device and (b) the device coated with sensing material.

cooled down naturally. The product was filtered and washed with deionized water, then dried at 80 °C overnight. The surfactant template was removed at 550 °C for 5 h to obtain the pure mesoporous silica SBA-15.

We prepared the sensing materials of MgO-SBA-15 by the same method. The detailed procedure was as follows: 2 g P123 was dissolved in 60 ml HCl solution at room temperature. Then, different molar ratio $Mg(NO_3)_2{\cdot}6H_2O$ was added to the former solution and stirred for 0.5 h. Next, 4.25 g tetraethyl orthosilicate (TEOS) was added dropwise under stirring at 40 °C for 24 h. The final aqueous solution was transferred into a Teflon-lined stainless steel autoclave, and treated hydrothermally at 100 °C for 24 h. Subsequently, the autoclave was cooled down naturally. The product was filtered and washed with deionized water, then dried at 80 °C overnight. The surfactant template was removed at 550 °C for 5 h. The MgO-SBA-15 samples were obtained and the products were designated as MgO-SBA-15(*R*), where *R* was the molar ratio of MgO to SBA-15. In our experiment, the value of *R* was 0.1, 0.3, 0.6, 1.0 and 1.5, respectively, for five MgO-SBA-15.

2.2. Sensor fabrications

The structure of the humidity sensor has been reported elsewhere [32,33]. The main processes were as follows: a ceramic substrate with two Ag–Pd interdigital electrodes with five fingers was selected for fabricating the humidity sensor. First, the powder sample was ground into paste with deionized water, and then the paste was spin-coated on the substrate. A positive film was coated on the sensing film to prevent the powder sample from being polluted. Fig. 1 shows the photograph of the blank device and the device coated with sensing material. Finally, the impedance-type humidity sensor was placed into 100%RH vapor aged with a voltage AC 1 V for 24 h.

2.3. Method of characterization

The XRD patterns of powder were obtained with a Bruker D8 Advance X-ray diffractometer using Cu Kα radiation at 40 kV and 40 mA. The nitrogen adsorption–desorption isotherm measurement was performed on a Micromeritics ASAP 2010 volumetric adsorption analyzer at the temperature of liquid nitrogen. The Fourier transform infrared (FTIR) spectra were recorded with Perkin-Elmer spectrometer, using KBr pellets whose thickness was about 1.3 mm. Each spectrum was collected at room temperature under the atmospheric pressure with a resolution of 4 cm^{-1}. The photograph of these devices was obtained by MEIJI three-dimensional microscope. The characteristic curves of humidity sensitivity were measured with the ZL-5 model LCR analyzer. The operation voltage was AC 1 V and the operation frequency was alterable. The controlled-humidity environment was achieved by releasing super-saturation aqueous solutions of different salts of LiCl, $MgCl_2$, $Mg(NO_3)_2$, NaCl, KCl, and KNO_3 in a closed glass vessel at room temperature (20 °C), which yielded 11%, 33%, 54%, 75%, 85% and 95% relative humidity, respectively.

3. Results and discussion

3.1. Structure and morphology

Fig. 2 gives the low-angle XRD pattern and the wide-angle XRD patterns of MgO-SBA-15(*R*). From the low-angle XRD patterns (Fig. 2a), all the curves can be observed in the three peaks attributed to (1 0 0), (1 1 0) and (2 0 0) of SBA-15. The intensity of these peaks decreased as the ratio of MgO increased. That means all the samples of MgO-SBA-15(*R*) have mesoporous structures, and the introduction of MgO do not destroy the mesoporous structure of SBA-15. The decrease of intensity indicated that the grade of the mesoporous structure was decreased. This can be confirmed by N_2 adsorption–desorption characterization. Fig. 2b shows the wide-angle XRD patterns of MgO-SBA-15(*R*). A broad peak centered at 22.2° of 2θ was observed for all the samples, indicating that the pore wall of SBA-15 and MgO-SBA-15(*R*) was amorphous. This result was in accordance with the low-angle patterns. When the ratio of MgO was low, we could not obtain the characteristic peak of MgO. When the ratio was up to 1.0, the diffraction peaks that appeared at $2\theta = 42.8°$ and 62.4° corresponded to the (2 0 0) and (2 2 0) of MgO, respectively.

In order to investigate the mesoporous structure of SBA-15 and MgO-SBA-15 further, the N_2 adsorption–desorption isotherm of pure SBA-15 and the representative isotherm curve of MgO-SBA-15($R = 0.6$, 1.0) are shown in Fig. 3. As shown in Fig. 3a, the curve belongs to type IV, indicating the mesoporous structure of SBA-15. When the MgO was assembled into mesoporous silica SBA-15, as shown in Fig. 3, the shape of type IV was still retained, illuminating the mesoporous structure preserved in the sample of MgO-SBA-15. This was consistent with the result of low-angle XRD. The testing

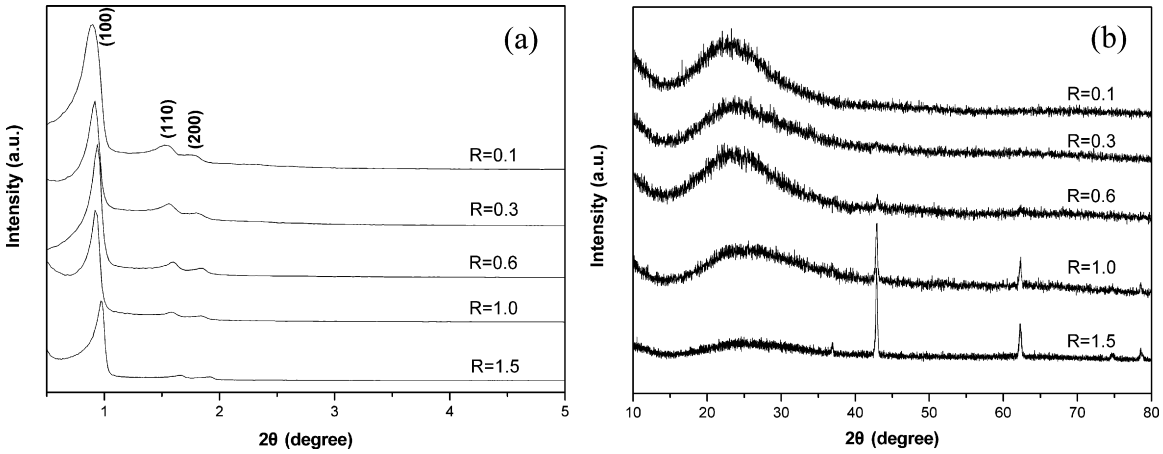

Fig. 2. XRD patterns MgO-SBA-15 samples: (a) low-angle XRD patterns and (b) wide-angle XRD patterns.

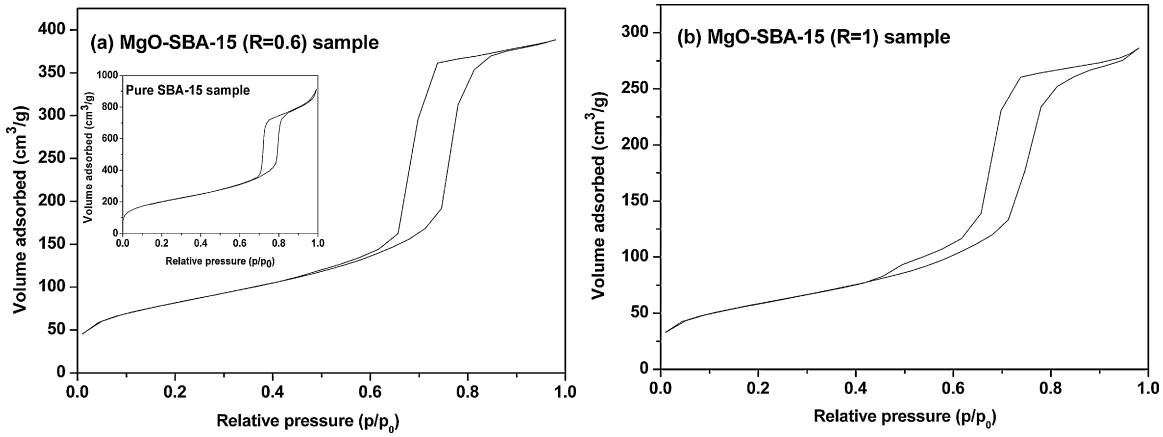

Fig. 3. Nitrogen adsorption–desorption isotherms of (a) MgO-SBA-15(R = 0.6) and (b) MgO-SBA-15(R = 1).

results show that the BET surface areas were decreased with the increase in MgO concentration. The BET surface areas for pure SBA-15, MgO-SBA-15(R = 0.6) and MgO-SBA-15(R = 1) are 728.99, 296.43 and 211.63 cm^2/g, respectively. The BJH pore diameter distributions that were calculated from desorption isotherms are shown in Fig. 4. The average pore width decreased too. The average pore width for MgO-SBA-15(R = 0.6) and MgO-SBA-15(R = 1) are 7.45 and 7.26 nm, respectively.

The transmission electron microscope (TEM) image of the MgO-SBA-15(R = 1) is shown in Fig. 5. TEM shows that the (1 0 0) direction still retains a regular hexagonal array of uniform channel characteristics (Fig. 5a). It suggested that MgO was formatted a smooth layer on the surface of SBA-15 due to the method was one-pot synthesis. The obtained result was similar to the reference result [37].

In order to confirm the element component, the sample MgO-SBA-15(R = 1) was investigated by X-ray photoelectron spec-

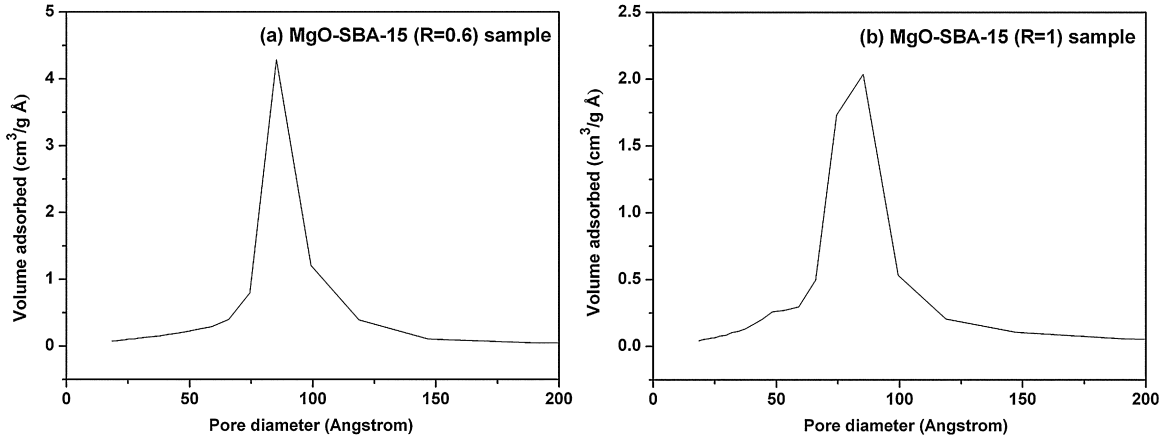

Fig. 4. Pore-size distribution of (a) MgO-SBA-15(R = 0.6) and (b) MgO-SBA-15(R = 1).

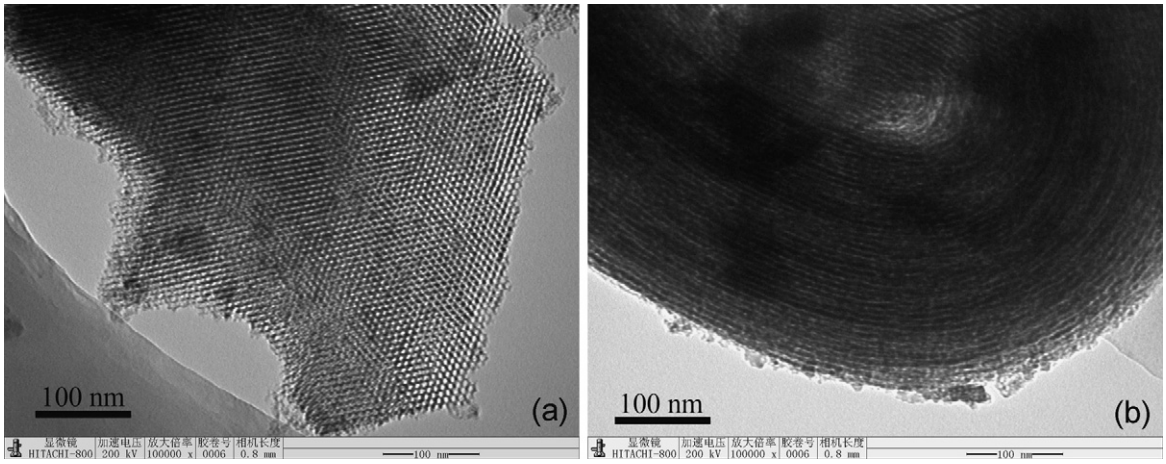

Fig. 5. TEM images of MgO-SBA-15(R = 1).

troscopic (XPS). As shown in Fig. 6, the binding energies of Mg*2p*, Si*2p* and O*1s* are 50.7, 102.7 and 532.2 eV, respectively. These results indicate the existence of the Mg–O and Si–O bond [38]. So the existence of MgO was confirmed by the XPS characterization.

IR spectra of SBA-15 and MgO-SBA-15(R) samples are shown in Fig. 7. The curves corresponded to the samples of SBA-15, MgO-SBA-15(0.1), MgO-SBA-15(0.3), MgO-SBA-15(0.6), MgO-SBA-15(1.0) and MgO-SBA-15(1.5), respectively. For mesoporous SBA-15, the peaks at 1093 and 808 cm^{-1} were attributed to the asymmetric stretching and symmetric modes of Si–O–Si lattice vibrations, respectively. The peaks at 1635 and 960 cm^{-1} were the characteristic peaks of Si–OH. After the assembly of MgO, the peak at 950 cm^{-1} became weak until it disappeared. But the characteristic peak of Si–OH at 1635 cm^{-1} became stronger with increasing MgO. This was due to the increasing of MgO content, and in increase in the number of water molecules interacting with the Si–O–Si of SBA-15 to form the surface hydroxyls. When the MgO ratio rose to 1.0, this peak began to decrease. This phenomenon may be caused by the surface hydroxyls beginning to release H^+, resulting in decreased amounts of the surface hydroxyls.

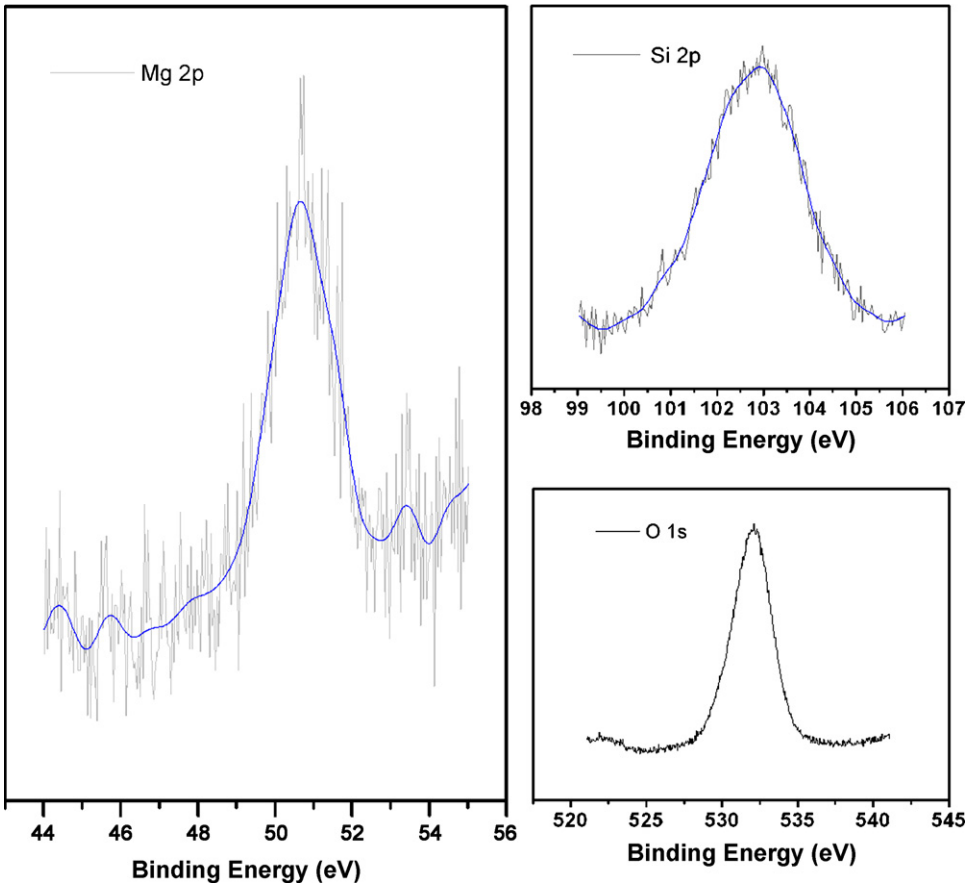

Fig. 6. XPS spectra of MgO-SBA-15(R = 1) of Mg*2p*, Si*2p* and O*1s*, respectively.

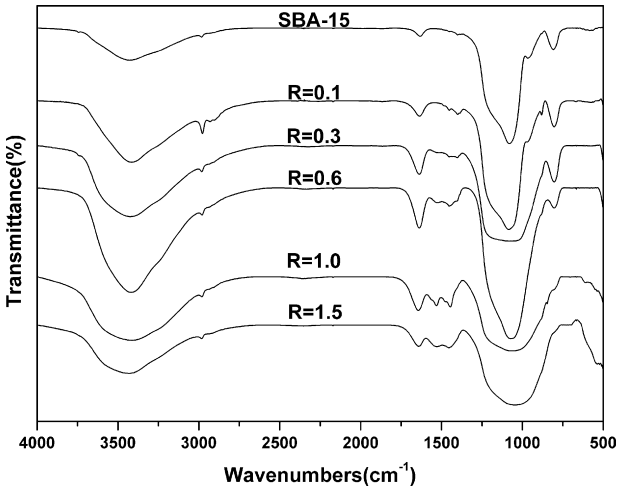

Fig. 7. IR spectra of pure SBA-15 and MgO-SBA-15.

3.2. Humidity-sensitive properties

The results of impedance measurements as a function of relative humidity at room temperature are shown in Fig. 8. The operation voltage was AC 1 V and the operation frequency was 100 Hz. At low humidity environment (11%RH), all the samples had very high impedance values. With the increasing of relative humidity, the impedance decreased rapidly. The greater the amount of MgO is, the lower impedance is. But when the amount of MgO reached $R = 1.5$, the impedance was higher than the others' in the indicated humidity environments. In our opinions, the reason is that the BET surface area and the inside pore was decreased by the excessive doping of MgO. It can be proven by the low-angle XRD characterization and N_2 adsorption. The results of Fig. 8 suggest that the curve of MgO-SBA-15($R = 1$) has the best linearity in the logarithmic scale. The impedance changes more than four magnitudes (10^4) from 11 to 95%RH. This sample exhibits the best humidity-sensitive properties, and therefore all the discussions below are focused on this sample. We selected it to evaluate the hysteresis, the optimal operation frequency, response-recovery time, and so on.

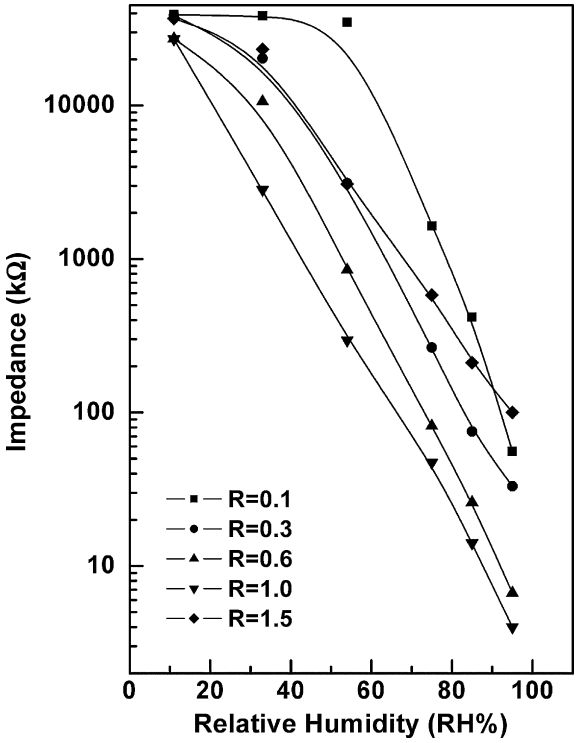

Fig. 8. Humidity-sensitive properties of MgO-SBA-15 samples.

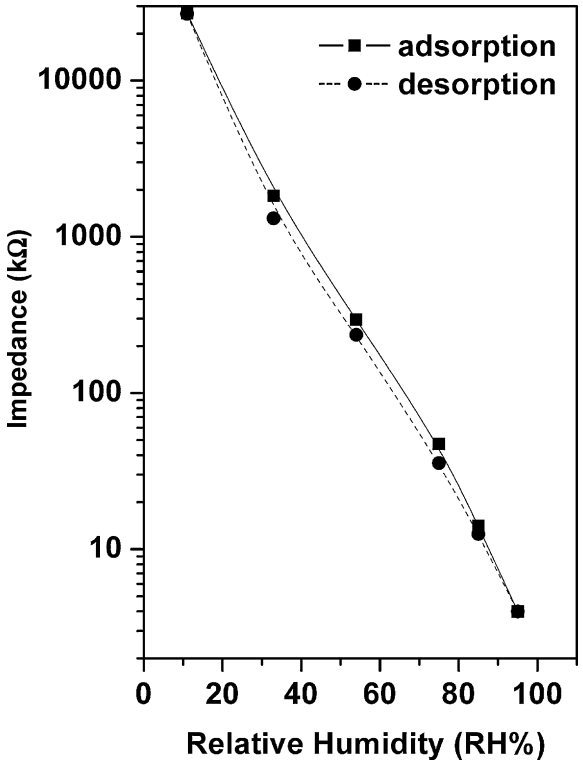

Fig. 9. Humidity hysteresis characteristic of MgO-SBA-15($R = 1$) sample.

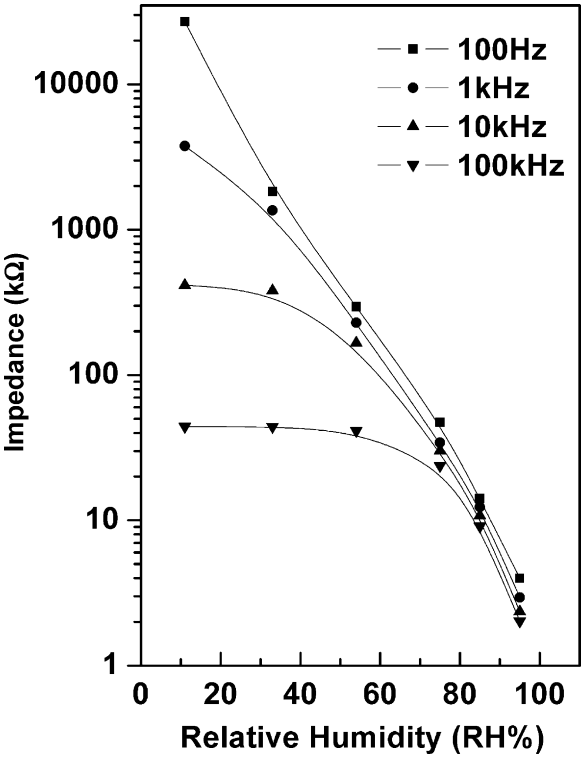

Fig. 10. Relationship of impedance and RH at different frequencies based on MgO-SBA-15($R = 1$) sample.

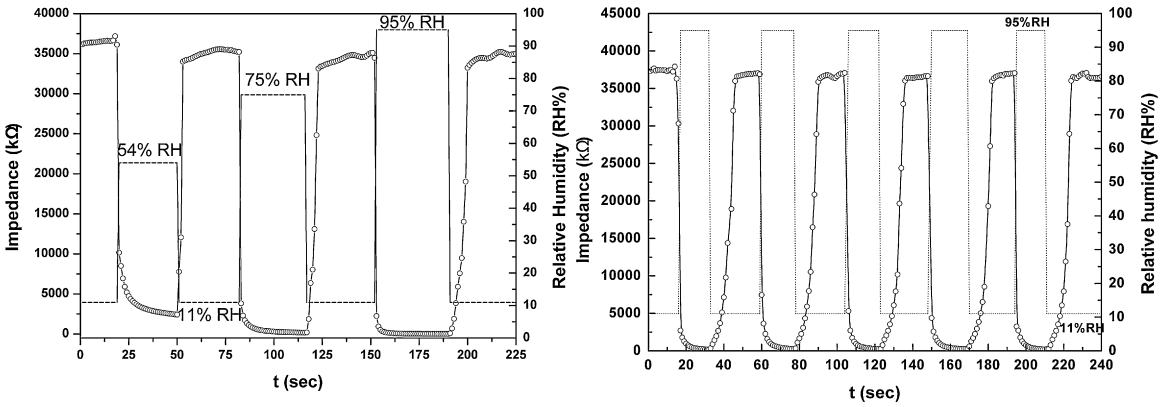

Fig. 11. Response and recovery curve of MgO-SBA-15($R = 1$) sample.

Hysteresis is one of the most important characteristics. It is defined as the maximum difference between the two outputs (adsorption and desorption cycle). Fig. 9 shows the humidity hysteresis curve. The solid line in the figure stands for the course from low to high relative humidity, corresponding to the adsorption process. The dashed line stands for the opposite direction, corresponding to the desorption process. The curve revealed that the largest humidity hysteresis was about 2% at 35%RH.

In order to investigate the internal relationship of operation frequency and impedance, we measured the impedance at different operation frequencies, and the curves are shown in Fig. 10. When the frequency was 100 Hz, the impedance decreased greatly with the increasing of relative humidity. When a higher frequency was used (1, 10 and 100 kHz), the range of impedance change decreased. Namely, at low humidity conditions, the frequency influence of the impedance was larger than when in the high humidity environment.

Fig. 11 shows the response and recovery curves measured in different humidity conditions. Fig. 11a shows the humidity sensor measured continuously in different humidity environments. We selected 11%RH as the initial humid environment and 54, 75 and 95%RH as the final one. The response and recovery were rather rapid. In order to investigate the response and recovery properties more clearly, Fig. 11b gave the humidity sensor measured in five periods from 11 to 95%RH, corresponding to water adsorption and desorption processes, respectively. The time taken by a sensor to reach 90% of the total impedance change is defined as the response and recovery time [39]. The impedance changed rapidly with the humidity environments' change. We can establish that this sensor has a very good response and recovery property.

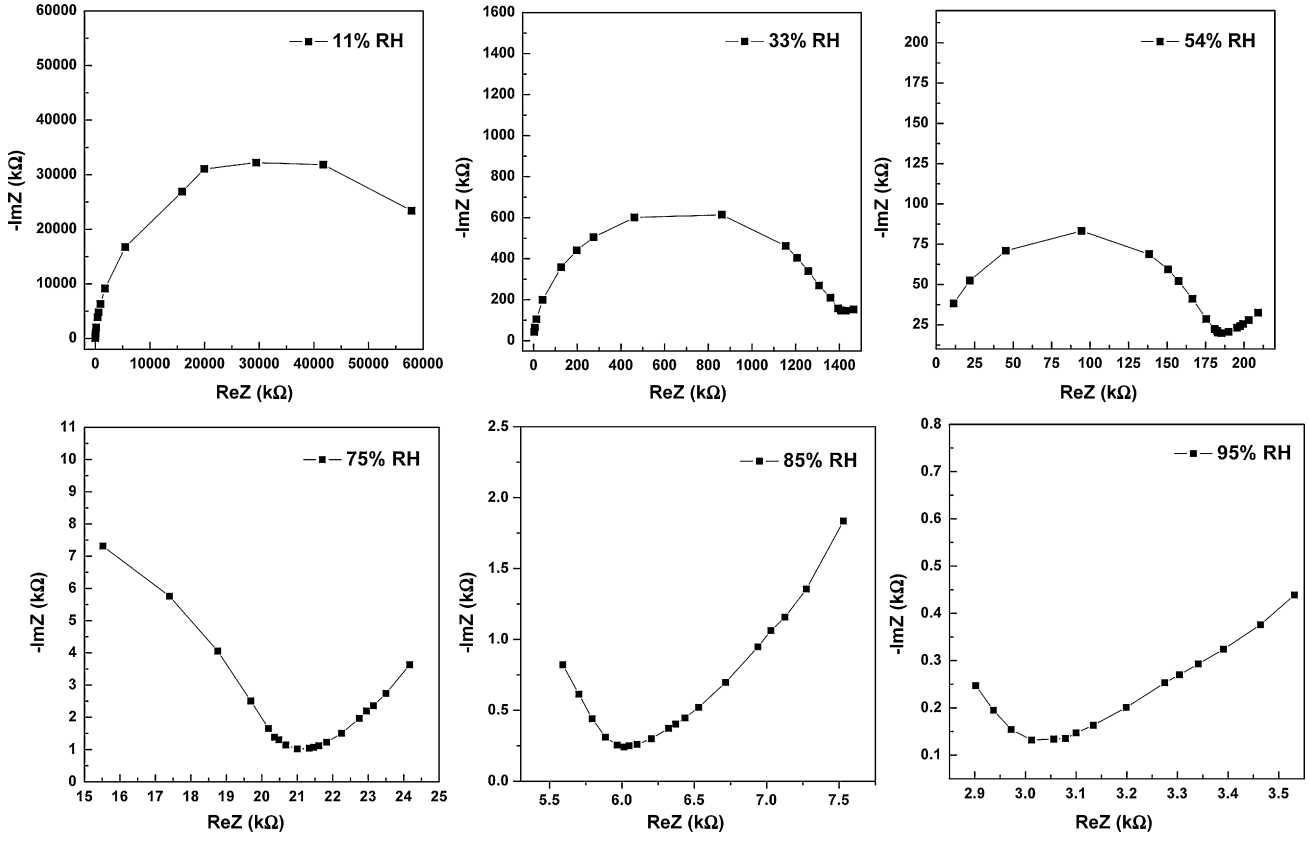

Fig. 12. Complex impedance plots of MgO-SBA-15($R = 1$) sample obtained from 20 Hz to 100 kHz, at room temperature.

The response time is about 10 s and the recovery time is about 20 s.

3.3. Discussion on sensing mechanism

In this section, we tried to discuss a possible humidity-sensitive process occurred on MgO-SBA-15 materials. The surface of the sensing material is usually covered with chemisorbed water layer after preparation in laboratory atmosphere. That means chemisorption already occurred even at 11%RH. Therefore, the ionic conduction exists even at extremely low humidity environments. Due to the low water vapor, the ionic conduction at room temperature is mainly due to the hopping of H^+ on the surface. So the sensor impedance is extremely high.

When the level of relative humidity grows, water vapor grows too. Since water molecules are polar, the negatively charged oxygen is electrostatic attached to the cations (Mg^{2+}, Si^{4+}) of the sensor materials. When the chemisorbed process finished, subsequent layers of water molecules are physically adsorbed. The physisorbed layers change with the outside relative-humidity environments. H^+ travels freely in the continuous water layers. Due of the electric fields in the chemisorbed water layer, the physisorbed water was dissociated as $2H_2O \leftarrow\rightarrow H_3O^+ + OH^-$. The charge transport occurs when H_3O^+ releases a proton to neighboring water molecules, which accept it while releasing another proton. This is known as Grotthuss chain reaction [40,41]. At high relative-humidity environments, liquid water condenses into the mesopores and electrolytic conduction [42] takes place in addition to proton transport.

In order to demonstrate the above analysis, we investigated complex impedance plots about the humidity sensor, based on MgO-SBA-15. Fig. 12 shows the typical complex impedance form 11 to 95%RH at room temperature, measured from 20 Hz to 100 kHz. It can be seen clearly from the figure that a semicircle was observed in complex impedance plot at low relative humidity, testified the existence of ionic conduction (H^+ hopping). When the relative humidity grows, the complex impedance plots consist of two parts: a semicircle at high frequency and a straight line at low frequency. That is caused by the H_3O^+ and H^+ traveling via the exchange of the Grotthuss chain mechanism. The appearance of a semicircle indicates an equivalent circuit consisting of parallel combination of resistance and capacitance components. The semicircle became ignorable under rather high humidity conditions during the selected frequency range. That is because the liquid water condensed into the mesopores and electrolytic conduction became active [42]. The sensor impedance decreased together with these processes. From the complex impedance plots analysis, we ascertained that the experimental results were in accordance with the theorized model.

4. Conclusions

MgO-SBA-15 was studied as a kind of humidity material. Its structure was characterized by low-angle XRD, wide-angle XRD, IR spectroscopy, N_2 adsorption–desorption, TEM and XPS. Though our investigation, the best molar ratio of MgO-SBA-15 was $R = 1$, and the impedance changed more than five orders of magnitude. We discussed a possible sensitive mechanism based on MgO-SBA-15 material, and complex impedance plots were also investigated.

Acknowledgments

This research was financially supported by National Natural Science Foundation of China (Granted No. 60971012) and Key Foundation Project from Education Ministry, China (Granted No. 108042).

References

[1] Y.F. Qiu, S.H. Yang, ZnO nanotetrapods: controlled vapor-phase synthesis and application for humidity sensing, Adv. Funct. Mater. 17 (2007) 1345–1352.
[2] C.L. Dai, M.C. Liu, F.S. Chen, C.C. Wu, M.W. Chang, A nanowire WO_3 humidity sensor integrated with micro-heater and inverting amplifier circuit on chip manufactured using CMOS-MEMS technique, Sens. Actuators B: Chem. 123 (2007) 896–901.
[3] J. Yang, K. Hidajat, S. Kawi, Synthesis of nano-SnO_2/SBA-15 composite as a highly sensitive semiconductor oxide gas sensor, Mater. Lett. 62 (2008) 1441–1443.
[4] C.T. Wang, C.L. Wu, Electrical sensing properties of silica aerogel thin films to humidity, Thin Solid Films 496 (2006) 658–664.
[5] P. Kapa, L. Pan, A. Bandhanadham, J. Fang, K. Varahramyan, W. Davis, H.F. Ji, Moisture measurement using porous aluminum oxide coated microcantilevers, Sens. Actuators B: Chem. 134 (2008) 390–395.
[6] G. Larsen, R.V. Ortiz, K. Minchow, A. Barrero, I.G. Loscertales, A method for making inorganic and hybrid (organic/inorganic) fibers and vesicles with diameters in the submicrometer and micrometer range via sol–gel chemistry and electrically forced liquid jets, J. Am. Chem. Soc. 125 (2003) 1154–1155.
[7] E. Moral, D.P. Fagg, E. Chinarro, J.C.C. Abrantes, J.R. Jurado, G.C. Mather, Impedance analysis of Sr-substituted $CePO_4$ with mixed protonic and p-type electronic conduction, Ceram. Int. 35 (2009) 1481–1486.
[8] J. Macan, A. Gajović, H. Ivanković, Porous zirconium titanate ceramics synthesized by sol–gel process, J. Eur. Ceram. Soc. 2 (2009) 691–696.
[9] M.V. Fuke, A. Vijayan, M. Kulkarni, R. Hawaldar, R.C. Aiyer, Evaluation of copolyaniline nanocomposite thin films as humidity sensor, Talanta 76 (2008) 1035–1040.
[10] J. Liu, M. Agarwal, K. Varahramyan, E.S. Berney, W.D. Hodo, Polymer-based microsensor for soil moisture measurement, Sens. Actuators B: Chem. 129 (2008) 599–604.
[11] Y. Li, Y. Chen, C. Zhang, T.X. Xue, M.J. Yang, A humidity sensor based on interpenetrating polymer network prepared from poly (dimethylaminoethyl methacrylate) and poly (glycidyl methacrylate), Sens. Actuators B: Chem. 125 (2007) 131–137.
[12] D. Patil, Y.K. Seo, Y.K. Hwang, J.S. Chang, P. Patil, Humidity sensitive poly(2,5-dimethoxyaniline)/WO_3 composites, Sens. Actuators B: Chem. 132 (2008) 116–124.
[13] M. Bognitzki, W. Czado, T. Frese, A. Schaper, M. Hellwig, M. Steinhart, A. Greiner, J.H. Wendorff, Nanostructured fibers via electrospinning, Adv. Mater. 13 (2001) 70–72.
[14] N. Camaioni, G. Casalbore-Miceli, Y. Li, M.J. Yang, A. Zanelli, Water activated ionic conduction in cross-linked polyelectrolytes, Sens. Actuators B: Chem. 134 (2008) 230–233.
[15] H. Aoki, Y. Azuma, T. Asaka, M. Higuchi, K. Asaga, K. Katayama, Improvement of response characteristics of TiO_2 humidity sensors by simultaneous addition of Li_2O and V_2O_5, Ceram. Int. 34 (2008) 819–822.
[16] S. Upadhyay, P. Kavitha, Lanthanum doped barium stannate for humidity sensor, Mater. Lett. 61 (2007) 1912–1915.
[17] S.M. Ke, H.T. Huang, H.Q. Fan, H.L.W. Chan, L.M. Zhou, Structural and electric properties of barium strontium titanate based ceramic composite as a humidity sensor, Solid State Ionics 179 (2008) 1632–1635.
[18] M. Bayhan, N. Kavasoğlu, A study on the humidity sensing properties of $ZnCr_2O_4$–K_2CrO_4 ionic conductive ceramic sensor, Sens. Actuators B: Chem. 117 (2006) 261–265.
[19] I.C. Cosentino, E.N.S. Muccillo, R. Muccillo, The influence of Fe_2O_3 in the humidity sensor performance of ZrO_2:TiO_2-based porous ceramics, Mater. Chem. Phys. 103 (2007) 407–414.
[20] J.J. Vijaya, L.J. Kennedy, G. Sekaran, B. Jeyaraj, K.S. Nagaraja, Effect of Sr addition on the humidity sensing properties of $CoAl_2O_4$ composites, Sens. Actuators B: Chem. 123 (2007) 211–217.
[21] W.F. Jiang, M. Jia, Y.S. Wang, L.Y. Li, X.J. Li, Accelerated resistive humidity sensing properties of silicon nanoporous pillar array, Thin Solid Films 517 (2009) 2994–2996.
[22] S.H. Xiao, H.J. Xu, J. Hu, W.F. Jiang, X.J. Li, Structure and humidity sensing properties of barium strontium titanate/silicon nanoporous pillar array composite films, Thin Solid Films 517 (2008) 929–932.
[23] P. Li, Y. Li, L.J. Hong, Y.S. Chen, M.Y. Yang, The electrical responses to humidity of a composite of polyaniline and polyelectrolyte, Mater. Chem. Phys. 115 (2009) 395–399.
[24] G. Fu, H. Chen, S.M. Hu, Z.Y. Liu, Humidity-sensitive properties and conductance mechanisms of SnO_2–K_2O–$LiZnVO_4$, Sens. Actuators B: Chem. 137 (2009) 17–20.
[25] Y. Aoki, H. Habazaki, T. Kunitake, Ion-conducting, sub-100 nm-thick film of amorphous hafnium silicate, Solid State Ionics, doi:10.1016/j.ssi.2009.02.016.
[26] C.T. Kresge, M.E. Leoniwics, W.J. Roth, J.C. Vartuli, J.S. Beck, Ordered mesoporous molecular sieves synthesized by a liquid crystal template mechanism, Nature 359 (1992) 710.
[27] J.S. Beck, J.C. Vartuli, W.J. Roth, M.E. Leonowicz, C.T. Kresge, K.D. Schmitt, C.T.W. Chu, D.H. Olson, E.W. Sheppard, S.B. McCullen, J.B. Higgins, J.L. Schlenker, A new family of mesoporous molecular sieves prepared with liquid crystal templates, J. Am. Chem. Soc. 114 (1992) 10834.
[28] D. Zhao, Q. Huo, J. Feng, B.F. Chmelka, G.D. Stucky, Nonionic triblock and star diblock copolymer and oligomeric surfactant syntheses of highly ordered, hydrothermally stable, mesoporous silica structures, J. Am. Chem. Soc. 120 (1998) 6024–6036.

[29] D. Zhao, J. Feng, Q. Huo, N. Melosh, G.H. Fredickson, B.F. Chmelka, G.D. Stucky, Triblock copolymer syntheses of mesoporous silica with periodic 50 to 300 Ångstrom pores, Science 279 (1998) 548–552.
[30] T. Yamada, H.S. Zhou, H. Uchida, M. Tomita, Y. Ueno, I. Honma, K. Asai, T. Katsube, Application of a cubic-like mesoporous silica film to a surface photovoltage gas sensing system, Micropor. Mesopor. Mater. 54 (2002) 269–276.
[31] T. Yamada, H.S. Zhou, H. Uchida, I. Honma, T. Katsube, Experimental and theoretical NO*x* physisorption analyses of mesoporous film (SBA-15 and SBA-16) constructed surface photovoltage (SPV) sensor, J. Phys. Chem. B 108 (35) (2004) 13341–13346.
[32] W.C. Geng, R. Wang, X.T. Li, Y.G. Zou, T. Zhang, J.C. Tu, Y. He, N. Li, Humidity sensitive property of Li-doped mesoporous SBA-15, Sens. Actuators B: Chem. 127 (2007) 323–329.
[33] T. Zhang, R. Wang, W.C. Geng, X.T. Li, Q. Qi, Y. He, S.J. Wang, Study on humidity sensing properties based on composite materials of Li-doped mesoporous silica A-SBA-15, Sens. Actuators B: Chem. 128 (2008) 482–487.
[34] J.C. Tu, R. Wang, W.C. geng, X.Y. Lai, T. Zhang, N. Li, N.Y. Yue, X.T. Li, Humidity sensitive property of Li-doped 3D periodic mesoporous silica SBA-16, Sens. Actuators B: Chem. 136 (2009) 392–398.
[35] V.V. Guliants, M.A. Carreon, Y.S. Lin, Ordered mesoporous and macroporous inorganic films and membranes, J. Membrane Sci. 235 (2004) 53–72.
[36] G. Li, X.S. Zhao, Characterization and photocatalytic properties of titanium-containing mesoporous SBA-15, Ind. Eng. Chem. Res. 45 (2006) 3569–3573.
[37] Y.M. Wang, Z.Y. Wu, Y.L. Wei, J.H. Zhu, In situ coating metal oxide on SBA-15 in one-pot synthesis, Micropor. Mesopor. Mater. 84 (2005) 127–136.
[38] N. Koshizaki, H. Umehara, T. Oyama, XPS characterization and optical properties of Si/SiO_2, Si/Al_2O_3 and Si/MgO co-sputtered films, Thin Solid Films 325 (1998) 130–136.
[39] S. Agarwal, G.L. Sharma, Humidity sensing properties of (Ba, Sr)TiO_3 thin films grown by hydrothermal–electrochemical method, Sens. Actuators B 85 (2002) 205–211.
[40] J.H. Anderson, G.A. Parks, The electrical conductivity of silica gel in the presence of adsorbed water, J. Phys. Chem. 72 (1968) 3662–3668.
[41] F.M. Ernsberger, The nonconformist ion, J. Am. Ceram. Soc. 11 (1983) 747–750.
[42] B.M. Kulwicki, Humidity sensors, J. Am. Ceram. Soc. 74 (1991) 697–708.

Biographies

Rui Wang received her BS, MS degree from the College of Electronics Science and Engineering, Jilin University, China in 2005 and 2007, respectively. She entered the PhD course in 2007, majored in microelectronics and solid state electronics, and engaged in novel sensing materials and humidity sensors.

Xiangwei Liu received his BS degree from College of Mechanical Engineering, Chongqing University, China in 2006. He received his MS degree from the College of Electronics Science and Engineering, Jilin University, China in 2009. He entered the PhD course in 2009, majored in microelectronics and solid state electronics, and engaged in novel sensing materials.

Yuan He received her BS, MS degree from the College of Electronics Science and Engineering, Jilin University, China in 2006 and 2008, respectively. She entered the PhD course in 2008, majored in microelectronics and solid state electronics, and engaged in novel sensing materials and humidity sensors.

Qing Yuan received her BS degree from the Department of Material Science in Jilin University, China in 2007. Presently she is a graduate student, majored in mesoporous materials.

Xiaotian Li is a professor of Department of Material Science in Jilin University. He received his BS, MS degree in Department of Electronic Science in Jilin University in 1989 and 1992, respectively. He obtained his PhD degree in the Department of Chemistry and State Key Laboratory of Inorganic Synthesis and Preparative Chemistry, Jilin University, in 2000. His main research interests are inorganic chemistry.

Geyu Lu received the BS degree in electronic sciences in 1985 and the MS degree in 1988 from Jilin University in China and the Dr Eng degree in 1998 from Kyushu University in Japan. Now he is a professor of Jilin University, China.

Tong Zhang received her MS degree in major of semiconductor materials in 1992, and PhD degree in the field of microelectronics and solid state electronics in 2001 from Jilin University. She was appointed a full professor in College of Electronics Science and Engineering, Jilin University in 2001. Now, she is interested in the field of sensing functional materials and gas sensors and humidity sensors.